Electronic Supplementary Material (ESI) for Soft Matter.
This journal is © The Royal Society of Chemistry 2017

Electronic Supplementary Information

Heat-Controlled Micropillar Array Device for Microsystems Technology

Núria Torras[a†§], Marcos Duque[a†], Carlos J. Camargo[a], Jaume Esteve[a]*, Antoni Sánchez-Ferrer[b]*

[a]Instituto de Microelectrónica de Barcelona, IMB-CNM (CSIC), Campus UAB, Bellaterra, E-08193 Barcelona, Spain. E-mail: jaume.esteve@imb-cnm.csic.es

[b]ETH Zurich, Department of Health Sciences & Technology, IFNH, Schmelzbergstrasse 9, CH-8092 Zurich, Switzerland. E-mail: antoni.sanchez@hest.ethz.ch

† The first two authors contributed equally to this study.

‡ Electronic supplementary information (ESI) available: thermoelastic, mechanical, IR temperature, time dependent and cyclic experiment; I-V curve; setups description; and LCE modelling.

§ Present address: Institute for Bioengineering of Catalonia (IBEC), Barcelona Institute of Science and Technology (BIST), Baldiri Reixac 10-12, E-08028 Barcelona Spain.

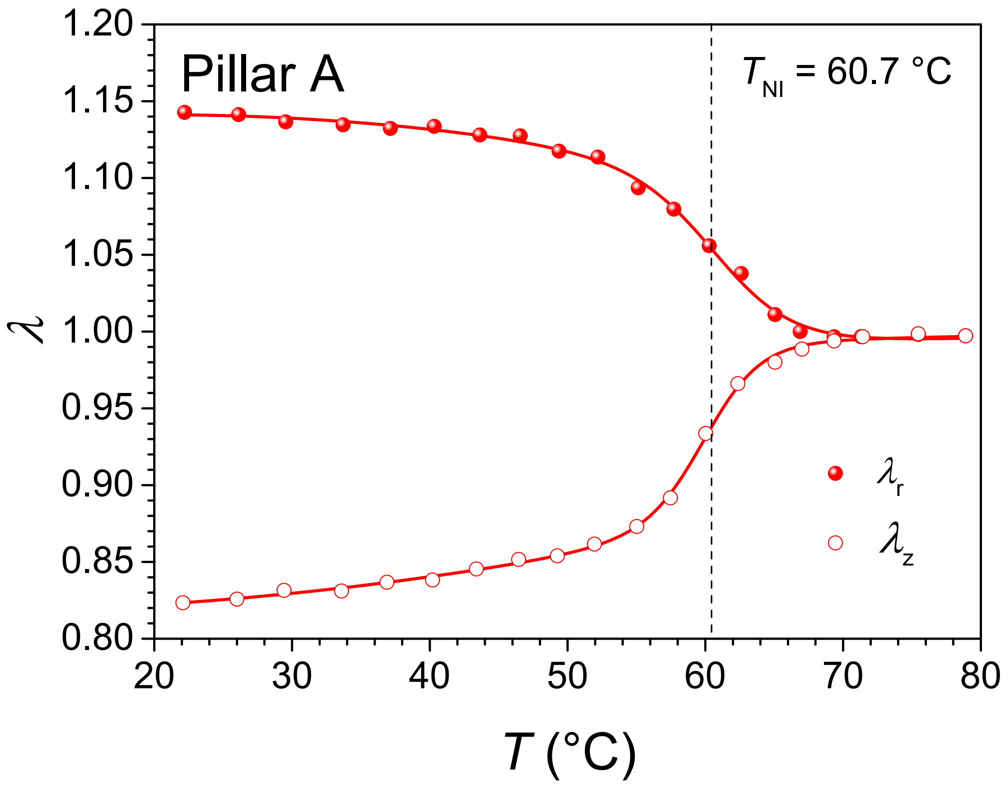

Figure ESI-1. Thermoelastic experiment on an oriented micropillar showing both the expansion along the axial direction (λ_z) and the contraction along the radial direction (λ_r). *Note:* the T_{NI} value corresponds to the inflection point of the heuristic fitting curve, showing a supercritical transition behavior of the two-dimensional prolate polydomain conformation of the LCE micropillar.

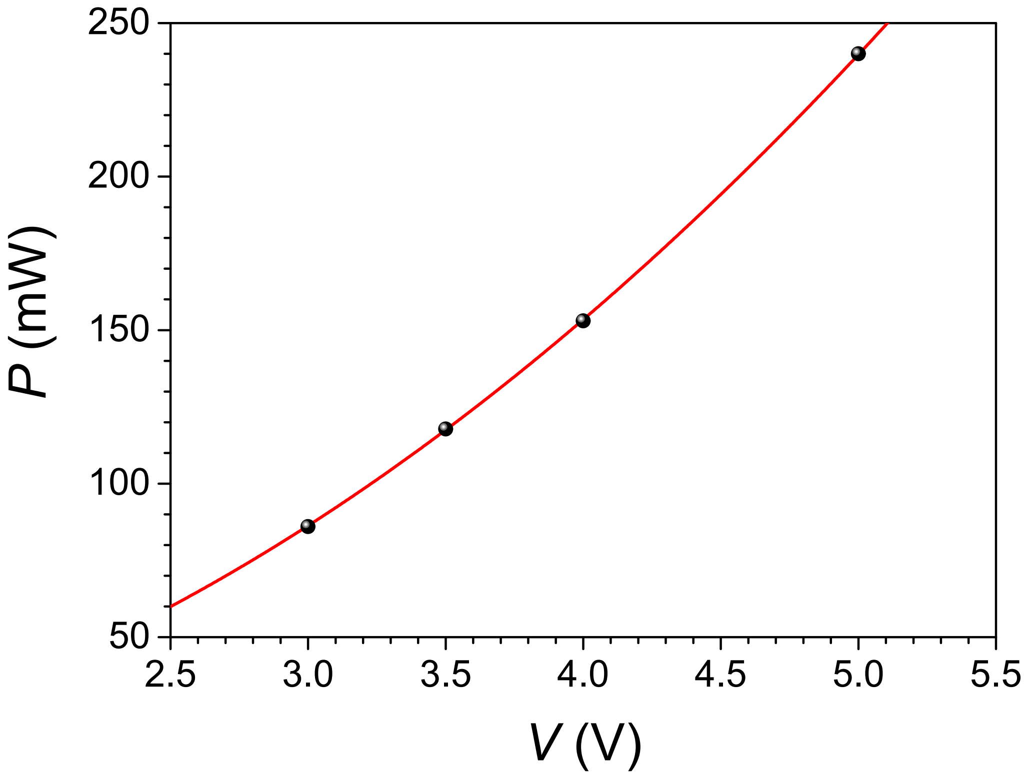

Figure ESI-2. I-V curves for the Au-microresistor. The measured resistance was 104.3 Ω ± 0.1 Ω.

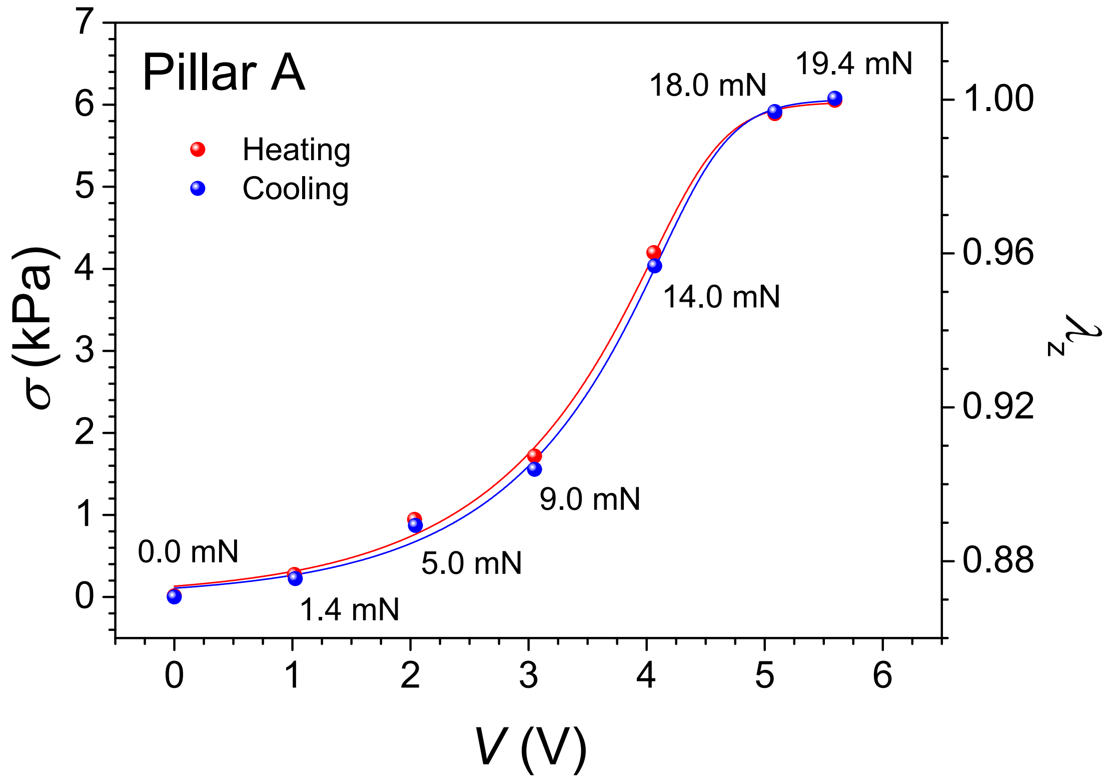

Figure ESI-3. Mechanical response of a LCE micropillar upon heating from room temperature and cooling to room temperature as function of the applied voltage (from 0 V to 5.5 V)

A)

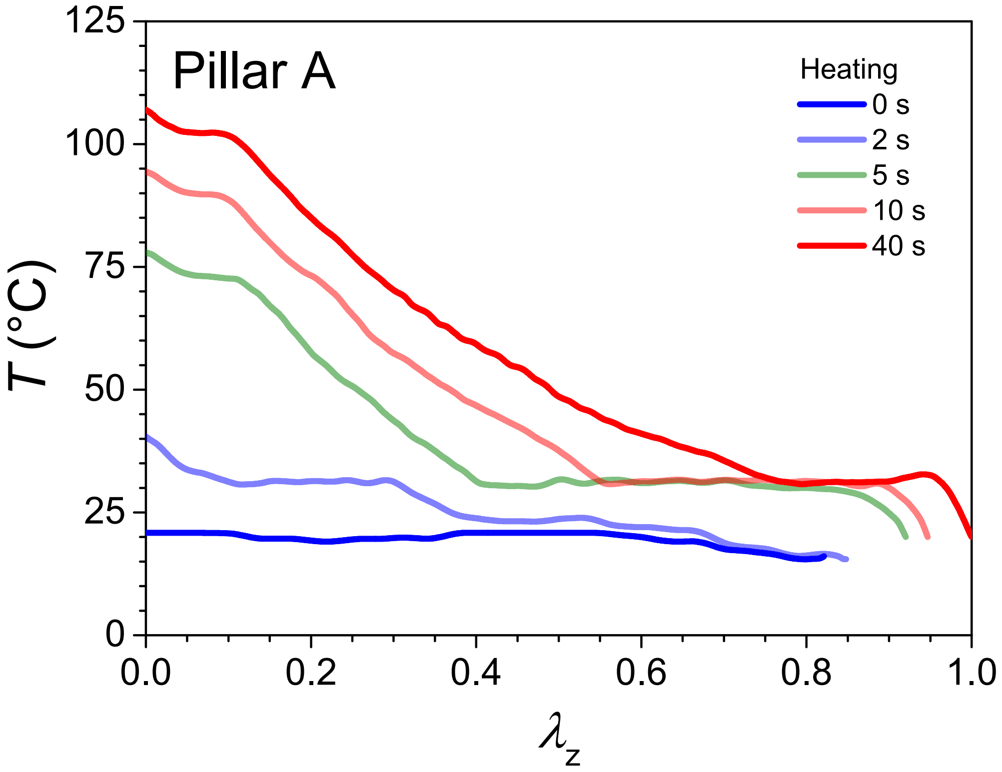

B)

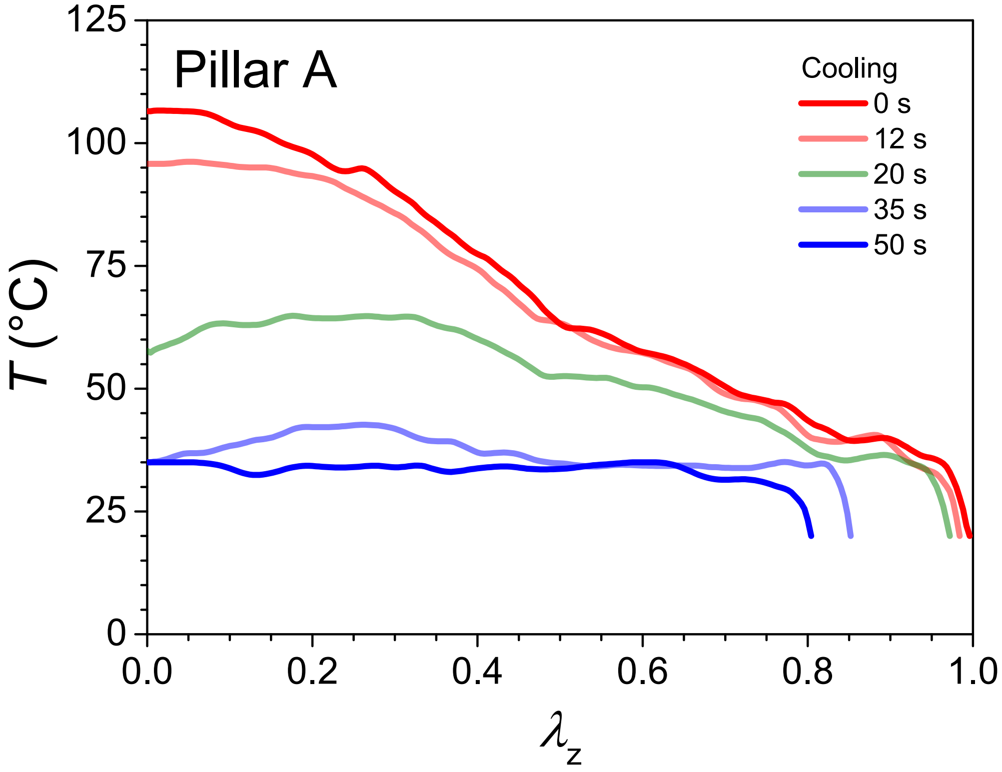

Figure ESI-4. Evolution of the temperature distribution along a LCE micropillar (A) upon heating, and (B) upon cooling using the IR camera.

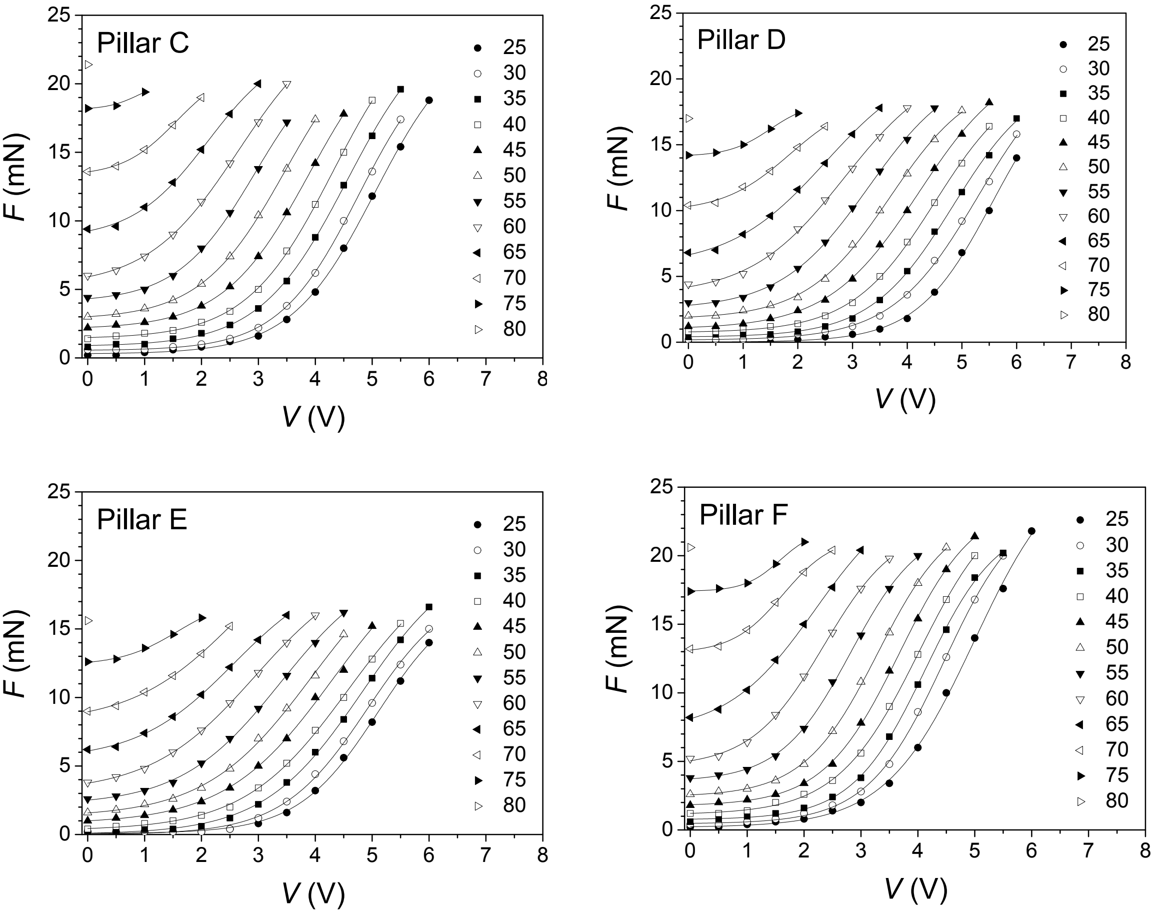

Figure ESI-5. Force (F) as function of the applied square-wave voltage (V) at different initial temperatures (T_0) for four more LCE micropillars.

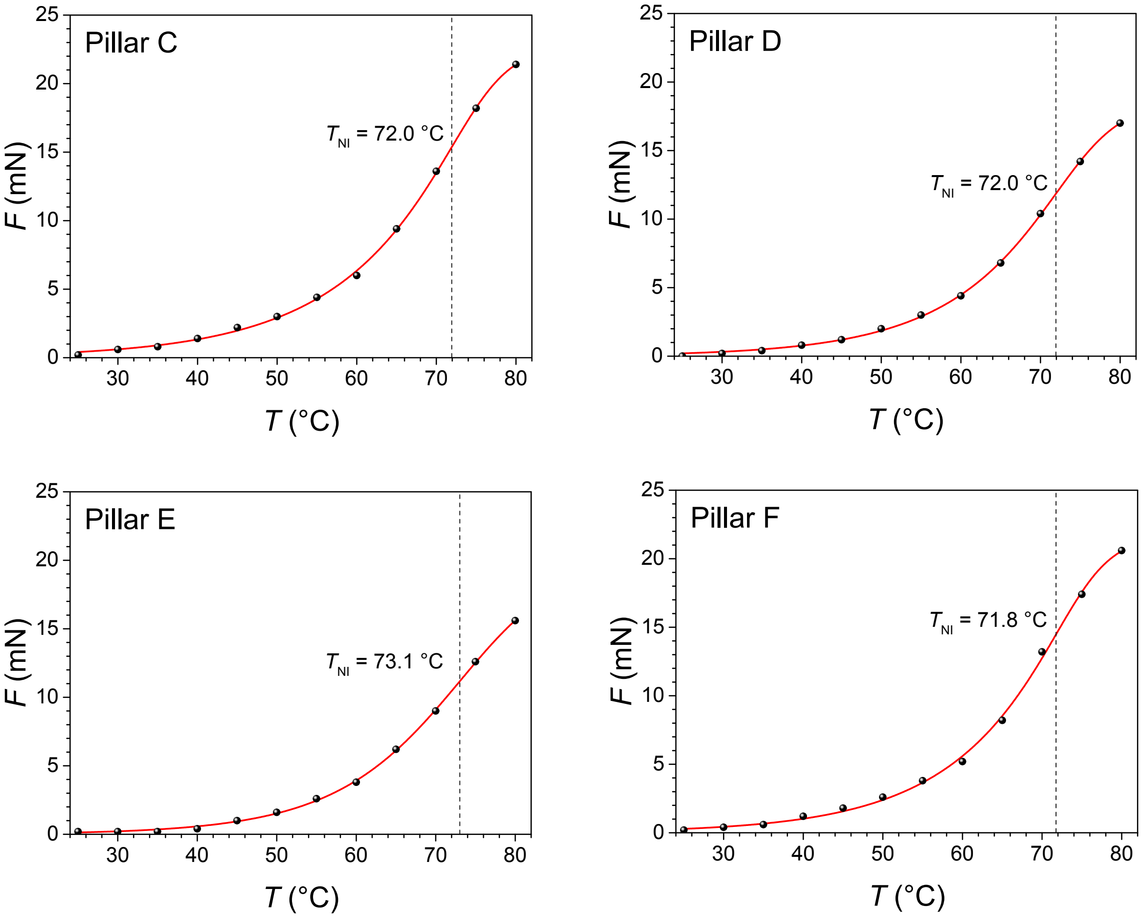

Figure ESI-6. Force (F) as function of temperature (T) for four more LCE micropillars. *Note:* the T_{NI} value corresponds to the inflection point of the heuristic fitting curve, showing an increase of *ca.* 10 °C in the transition temperature due to the ultrafast heating process.

Table ESI-1. Isotropization voltage values (V_{NI}) obtained from the fitting curves in Figure 4A (eq. 1) and Figure ESI-5, and the corresponding isotropization temperature (T_{NI}) obtained from the fitting curves in Figure 4B (eq. 2) and Figure ESI-6 for the five LCE micropillars at different initial temperatures (T_0).

	Pillar A		Pillar C		Pillar D		Pillar E		Pillar F	
T_0 (°C)	V_{NI} (V)	T_{NI} (°C)	V_{NI} (V)	T_{NI} (°C)	V_{NI} (V)	T_{NI} (°C)	V_{NI} (V)	T_{NI} (°C)	V_{NI} (V)	T_{NI} (°C)
25	5.13	68.5	5.05	68.4	5.56	70.4	5.10	69.7	4.99	71.1
30	4.88	69.5	4.76	68.2	5.29	71.0	4.92	70.1	4.46	69.5
35	4.63	70.2	4.56	69.4	4.84	70.1	4.82	71.9	4.13	68.9
40	4.19	69.5	4.31	70.1	4.51	70.4	4.57	72.1	4.02	70.2
45	3.93	70.1	3.90	70.0	4.21	71.3	4.31	73.3	3.68	70.2
50	3.55	70.3	3.47	70.2	3.69	70.9	3.95	73.6	3.29	70.2
55	2.99	69.7	2.95	70.0	3.29	71.8	3.40	73.0	2.82	70.2
60	2.45	69.5	2.65	71.7	2.85	72.8	2.95	73.6	2.35	70.7
65	2.47	73.1	2.11	72.4	2.51	74.3	2.57	74.9	2.20	73.4
70	1.62	75.0	1.56	73.9	1.86	75.1	2.63	80.2	1.63	74.5
75					1.50	78.2	1.57	78.6	1.58	77.9

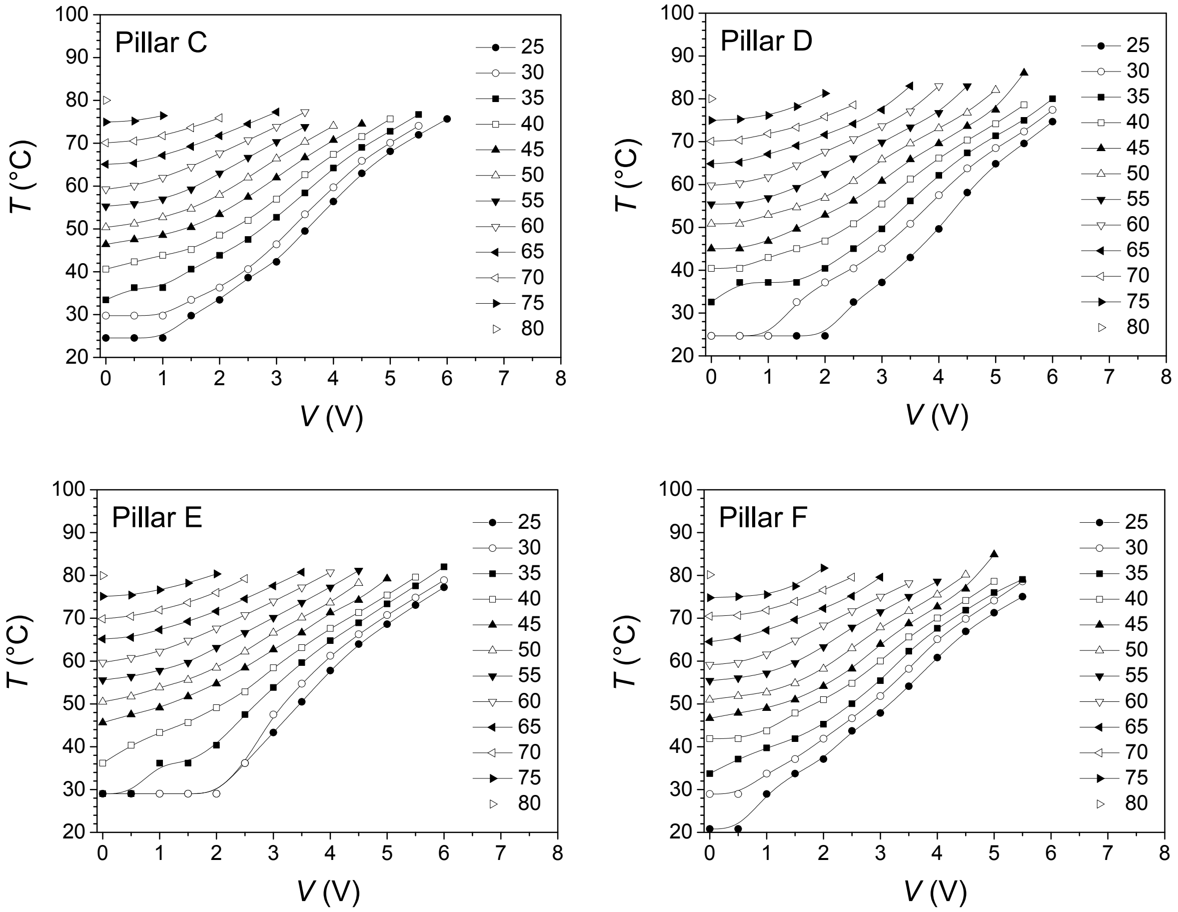

Figure ESI-7. Temperature (*T*) as function of the applied square-wave voltage (*V*) at different initial temperatures (T_0) for four more LCE micropillars.

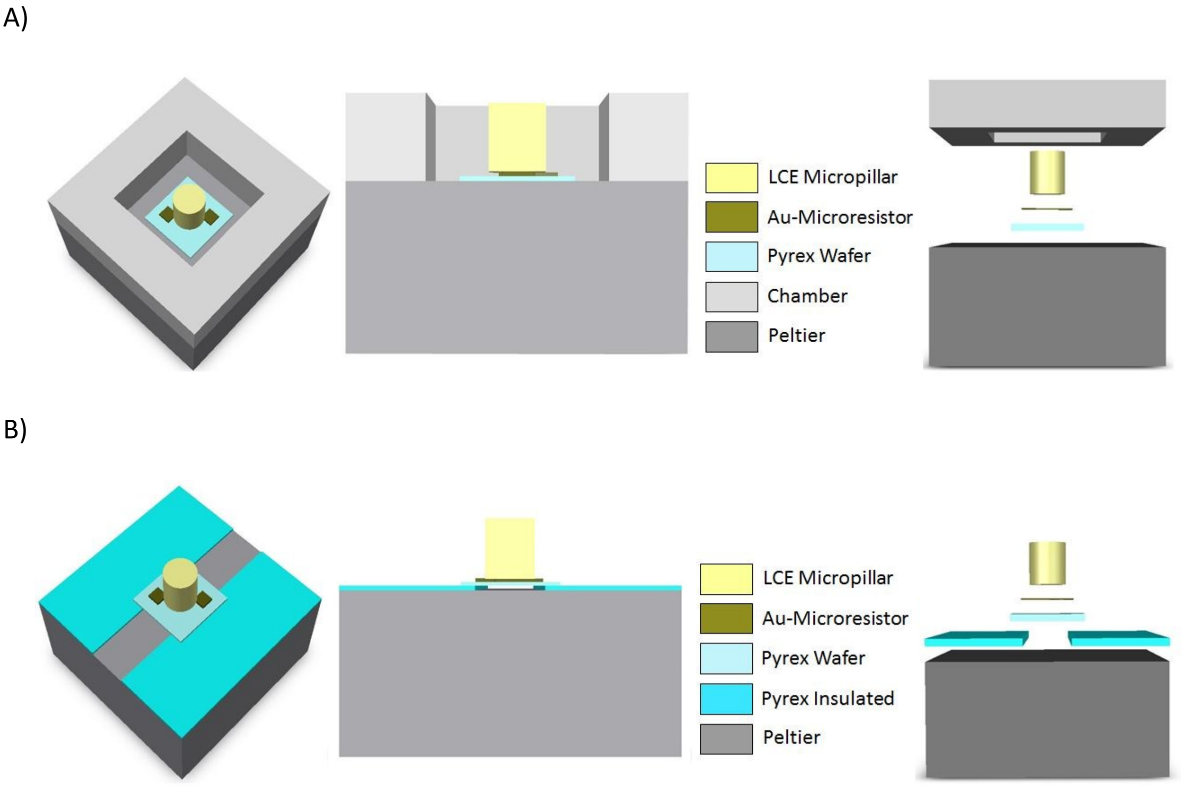

Figure ESI-8. (A) Setup 1 and 2: closed system where the temperature is controlled by a Peltier system in direct contact to the bottom Pyrex surface (“Closed Chamber/Peltier” experiments), or without controlling the temperature with the Peltier block (“Closed Chamber” experiments). (B) Setup 3: open system where the LCE microdevice is insulated from the Peltier-heating block (“Open Chamber” experiments).

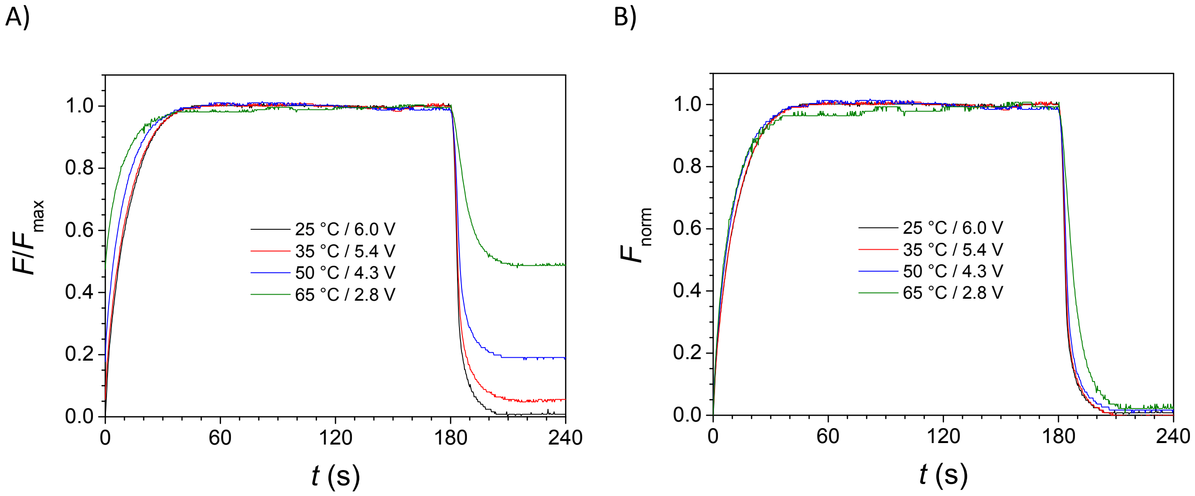

Figure ESI-9. (A) Relative force (F/F_{max}) and (B) normalized force (F_{norm}) evolution comparison upon applying different square-wave voltage values (V) (from 6.0 to 2.8 V) for 180 s at different initial temperatures (T_0) (from 25 to 65 °C), and after removal of the voltage ("Closed Chamber/Peltier" setup): **Setup 1.**

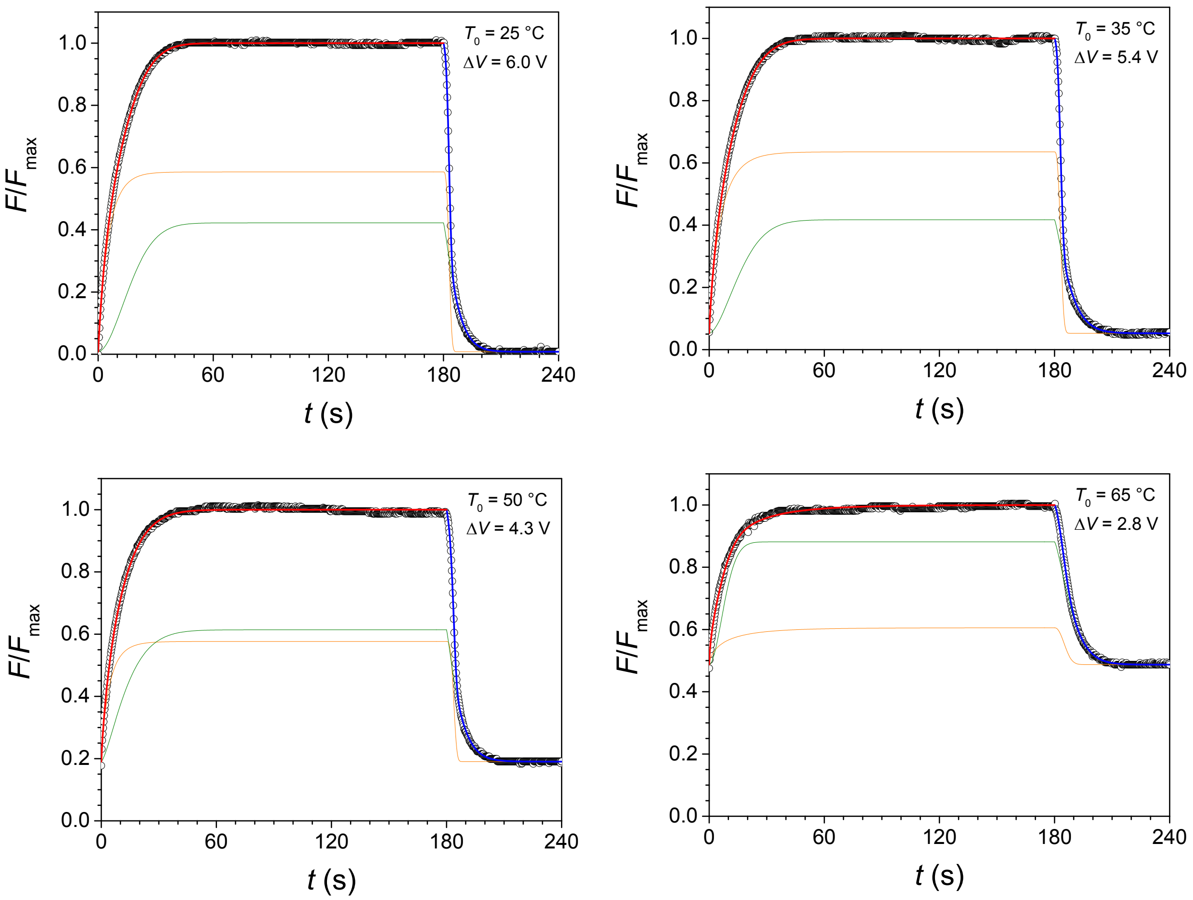

Figure ESI-10. Relative force (F/F_{max}) evolution upon applying different square-wave voltage values (V) (from 6.0 to 2.8 V) for 180 s at different initial temperatures (T_0) (from 25 to 65 °C), and after removal of the voltage, as well as the corresponding fitting curves for the heating and cooling processes ("Closed Chamber/Peltier" setup): **Setup 1.**

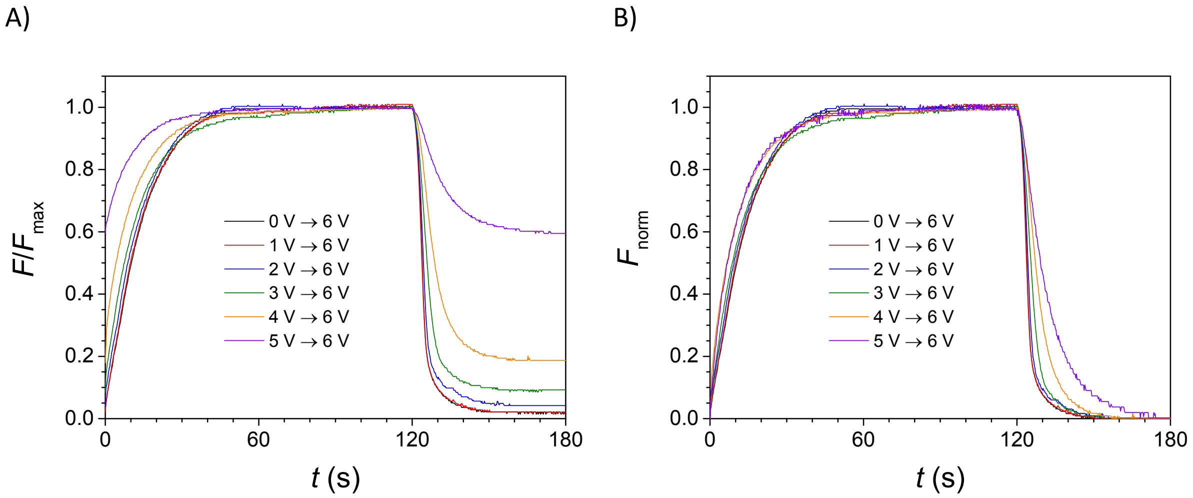

Figure ESI-11. (A) Relative force (F/F_{max}) and (B) normalized force (F_{norm}) evolution comparison upon applying different initial square-wave voltage values (V) (from 0 to 5 V) up to 6 V for 120 s at room temperature, and after coming back to the initial applied voltage (“Closed Chamber” setup): **Setup 2.**

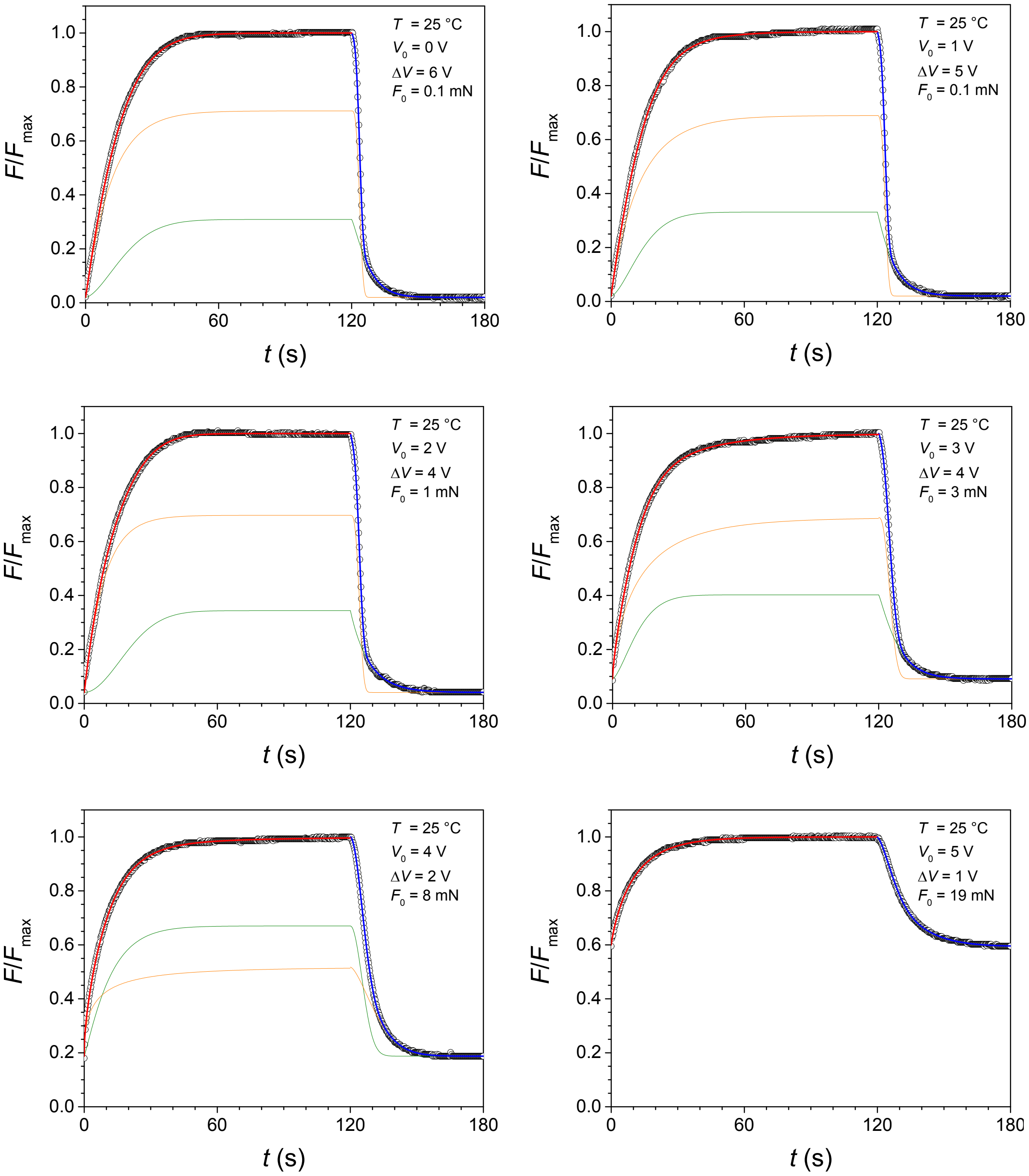

Figure ESI-12. Relative force (F/F_{max}) evolution upon applying different initial square-wave voltage values (*V*) (from 0 to 5 V) up to 6 V for 120 s at room temperature, and after coming back to the initial applied voltage, as well as the corresponding fitting curves for the heating and cooling processes ("Closed Chamber" setup): **Setup 2.**

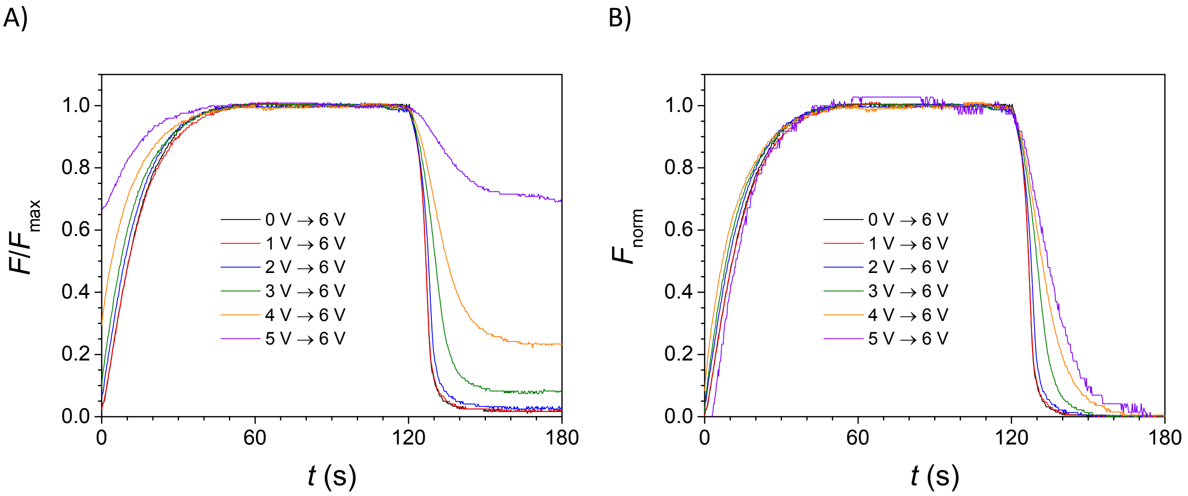

Figure ESI-13. (A) Relative force (F/F_{max}) and (B) normalized force (F_{norm}) evolution comparison upon applying different initial square-wave voltage values (V) (from 0 to 5 V) up to 6 V for 120 s at room temperature, and after coming back to the initial applied voltage ("Open Chamber" setup): **Setup 3.**

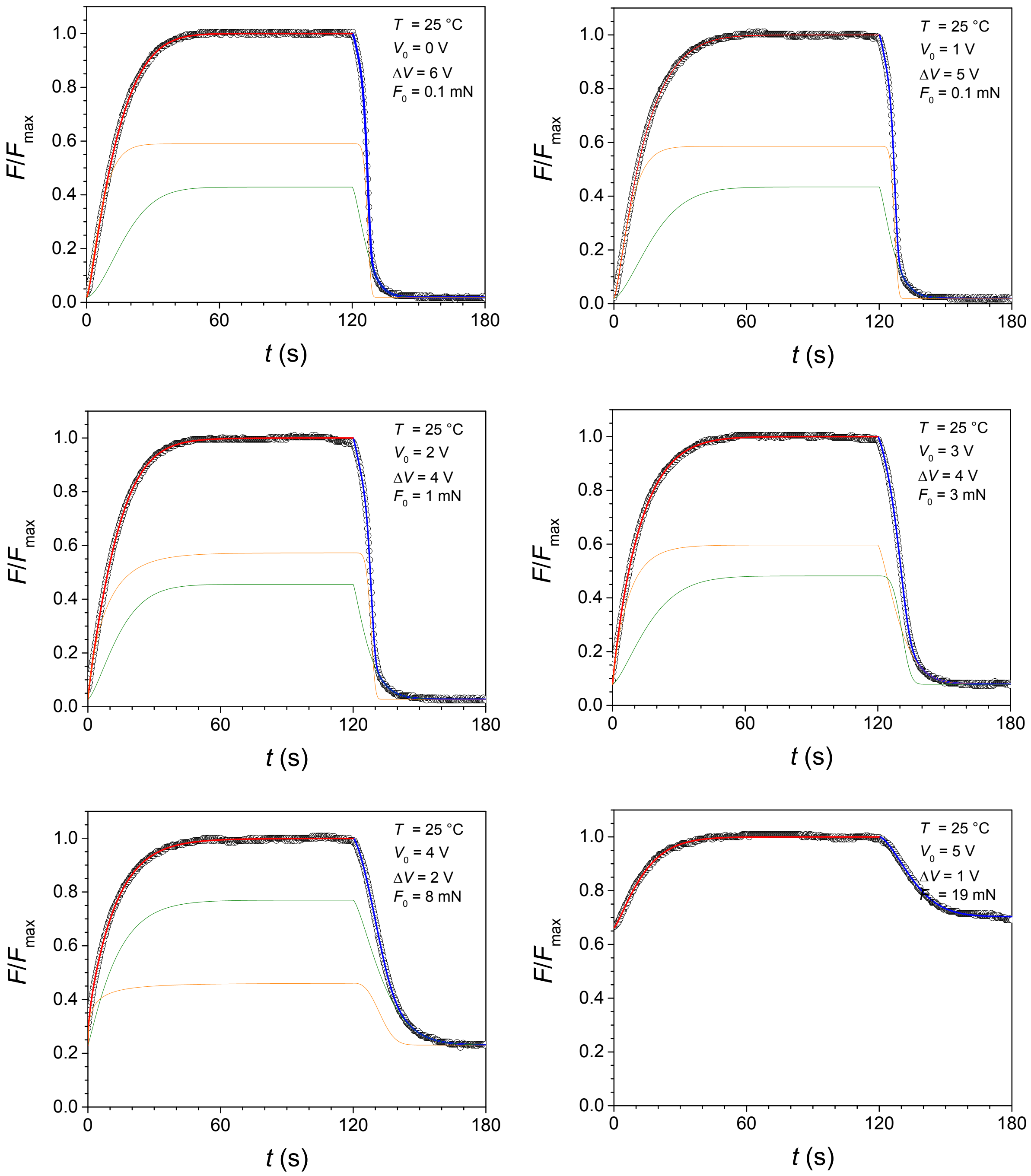

Figure ESI-14. Relative force (F/F_{max}) evolution upon applying different initial square-wave voltage values (V) (from 0 to 5 V) up to 6 V for 120 s at room temperature, and after coming back to the initial applied voltage, as well as the corresponding fitting curves for the heating and cooling processes ("Open Chamber" setup): **Setup 3.**

Table ESI-2. Lifetime (τ), stretched exponent (β) and percentages for the fast and slow processes upon heating and cooling (“Closed Chamber/Peltier” setup): **Setup 1.**

T_0 (°C)	τ_{h1} (s)	τ_{h2} (s)	τ_{c1} (s)	τ_{c2} (s)
25	5.3	19.9	3.4	7.3
35	5.9	18.9	3.6	8.8
50	4.2	15.2	4.2	7.3
65	8.7	9.7	6.5	10.2

T_0 (°C)	β_{h1}	β_{h2}	β_{c1}	β_{c2}
25	0.95	1.83	3.20	1.24
35	0.86	1.67	2.95	1.25
50	0.87	1.37	3.38	1.17
65	0.65	1.85	2.25	1.35

T_0 (°C)	μ	$1 - \mu$	bkg
25	58%	41%	1%
35	58%	36%	5%
50	39%	42%	19%
65	12%	39%	49%

Table ESI-3. Lifetime (τ), stretched exponent (β) and percentages for the fast and slow processes upon heating and cooling ("Closed Chamber" setup): **Setup 2.**

T_0 (°C)	τ_{h1} (s)	τ_{h2} (s)	τ_{c1} (s)	τ_{c2} (s)
25	11.8	20.5	4.1	8.1
25	13.0	16.0	4.0	7.6
30	12.7	14.3	4.6	8.5
44	12.7	12.9	6.0	9.2
58	12.2	10.3	7.2	14.0
70		10.5		12.6

T_0 (°C)	β_{h1}	β_{h2}	β_{c1}	β_{c2}
25	1.03	1.62	3.31	1.21
25	0.94	1.56	3.15	1.08
30	1.04	1.20	3.21	0.98
44	0.73	1.47	2.51	1.14
58	1.02	0.90	2.04	1.56
70		0.87		1.26

T_0 (°C)	μ	1 - μ	bkg
25	69%	29%	2%
25	67%	31%	2%
30	66%	30%	4%
44	60%	31%	9%
58	48%	33%	19%
70	0%	40%	60%

Table ESI-4. Lifetime (τ), stretched exponent (β) and percentages for the fast and slow processes upon heating and cooling ("Open Chamber" setup): **Setup 3.**

T_0 (°C)	τ_{h1} (s)	τ_{h2} (s)	τ_{c1} (s)	τ_{c2} (s)
25	7.7	20.0	7.5	7.3
25	8.3	20.6	7.5	7.4
30	8.7	16.0	8.2	8.6
44	7.3	19.0	11.3	11.9
58	2.9	13.6	15.5	14.0
70		14.5		17.8

T_0 (°C)	β_{h1}	β_{h2}	β_{c1}	β_{c2}
25	1.30	1.69	1.43	5.84
25	1.30	1.54	1.31	5.67
30	0.85	1.41	1.23	5.56
44	0.95	1.40	1.36	3.77
58	0.48	1.11	1.38	2.68
70		1.26		1.59

T_0 (°C)	μ	1 - μ	bkg
25	41%	57%	2%
25	41%	57%	2%
30	43%	54%	3%
44	52%	40%	8%
58	54%	54%	23%
70	0%	34%	66%

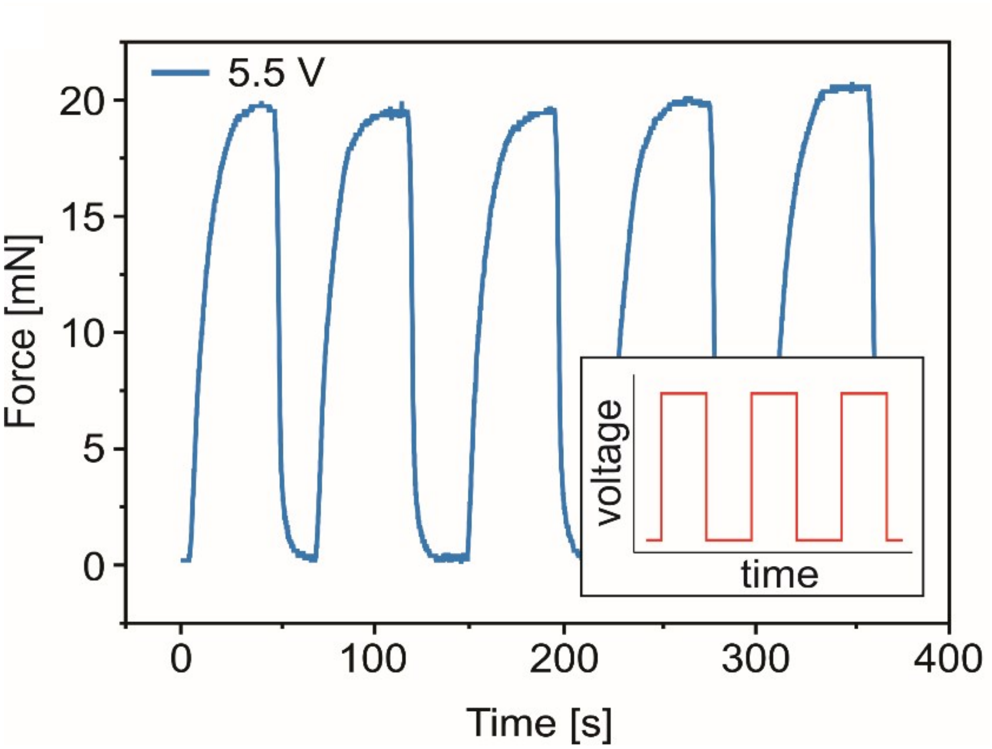

Figure ESI-15. Voltage-controlled response of a single LCE micropillar during five on-off actuation cycles when 5.5 V were applied. A maximum force of *F* = 19.4 mN ± 0.4 mN was obtained, with full reversibility.

LCE Modelling

Both, the heat and the temperature spatial distribution along the micropillars were obtained by quantitative and qualitative finite element simulations using COMSOL Multiphysics software (Burlington, MA, USA, www.comsol.com), coupling both Heat Transfer and Electric Currents modules. All the elements in the model, the microresistor, the micropillar, and both the Pyrex glass and aluminum substrates were modeled by a 3D element, using a free tetrahedral mesh with a minimum mesh size of 70 µm and a growing rate of 1.45.

First, we have studied the heating of the material as function of the applied voltage to the microresistor by means of *Joule effect*, and by applying a square-wave electrical voltage of 6 V between the terminals of the microresistor for 3 min. At that point, an increase in the temperature due to the current through the resistor should be considered resulting in a variation in the resistivity of the material, which was linearized as function of the temperature for each time point.

The simulated LCE microdevice (Au-microresistor and LCE micropillar) was placed on top of an aluminum plate that emulates the same heat distribution at the bottom side of the resistor as exists when the Peltier is switched on and working under real operating conditions, in order to ensure the same heat flux distribution in the microdevice placed in a setup.

In order to translate such temperature gradient from the resistor to the LCE micropillar, the Heat Transfer module for solids was applied taking into account the main properties of the LCE material and their variations when T_{NI} is reached. To that, Fourier's law, $\vec{q} = -\lambda \nabla T$, that reflects an existing proportionality between the flux of energy, $\vec{q}$, and the temperature gradient between both sample ends, ∇T, which depends, at the same time, on the thermal conductivity of the material, λ, was used. Applying the Taylor expansion in cylindrical coordinates (which better fits the geometry of the micropillars), and considering the first thermodynamic law (conservation of energy), we can obtain the generic expression for the thermal conductivity of our system in the differential form

$$\frac{1}{r}\frac{\partial}{\partial r}\left(\lambda\frac{\partial T}{\partial r}\right) + \frac{1}{r^2}\frac{\partial}{\partial \phi}\left(\lambda\frac{\partial T}{\partial \phi}\right) + \frac{\partial}{\partial z}\left(\lambda\frac{\partial T}{\partial z}\right) + \dot{q} = \rho C p \Delta T$$

Eq. ESI-1

expression that establishes the thermal balance in terms of heat flux, and the generated and stored heat.

Parameters such as the enthalpy, ΔH, the heat capacity, C_p, and the working range of temperatures of the material were experimentally-determined from the DSC measurements. The equation below shows the C_p at a constant pressure as function of the temperature in a Gaussian form.

$$Cp = 2.11421 + 0.2394 \cdot e^{\left(-0.5 \cdot \frac{T - 337.54329}{6.39322^2}\right)} \qquad \textit{Eq. ESI-2}$$

Finally, thermal dissipation losses due to the direct contact between different elements, *e.g.*, LCE micropillar base and Au-microresistor, Au-microresistor and Pyrex, and Pyrex and aluminum substrate were considered (**Figure ESI-modelling-1A**). Additionally, convection effects were taken into account for all surfaces which are supposed to be in contact with the surrounding air, both the substrate and the top and lateral surfaces of the LCE micropillar (**Figure ESI-modelling-1B**).

A)

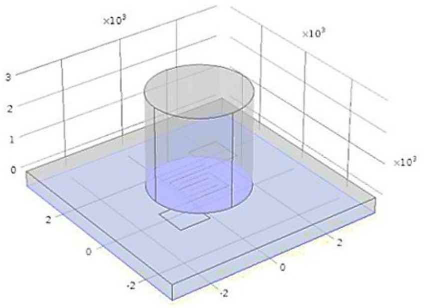

B)

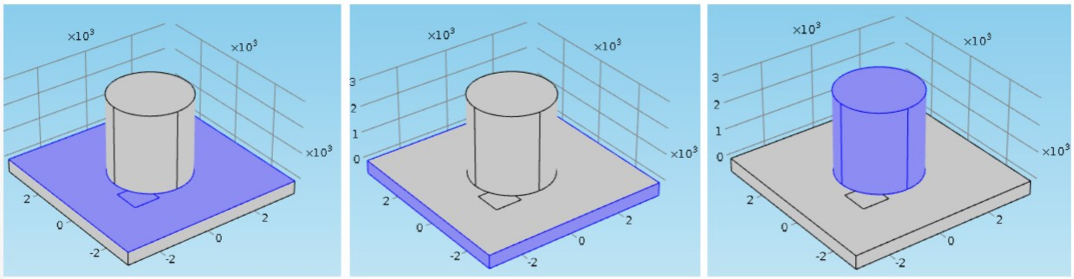

Figure ESI-modelling-1. Thermal dissipation losses considered in the model due to (A) conduction and (B) convection effects.

Figure ESI-modelling-2 shows the modelling results by coupling the electric and heat transfer analysis. As expected, the higher temperature values (118 °C) are in the region where the Au-microresistor and the LCE micropillar are in contact. There is a uniform heat distribution along the pillar, which decreases along the micropillar vertical axis with a mean value of about 75 °C, and is enough for promoting the nematic-to-isotropic transition, as experimentally determined in previous thermoelastic experiments.

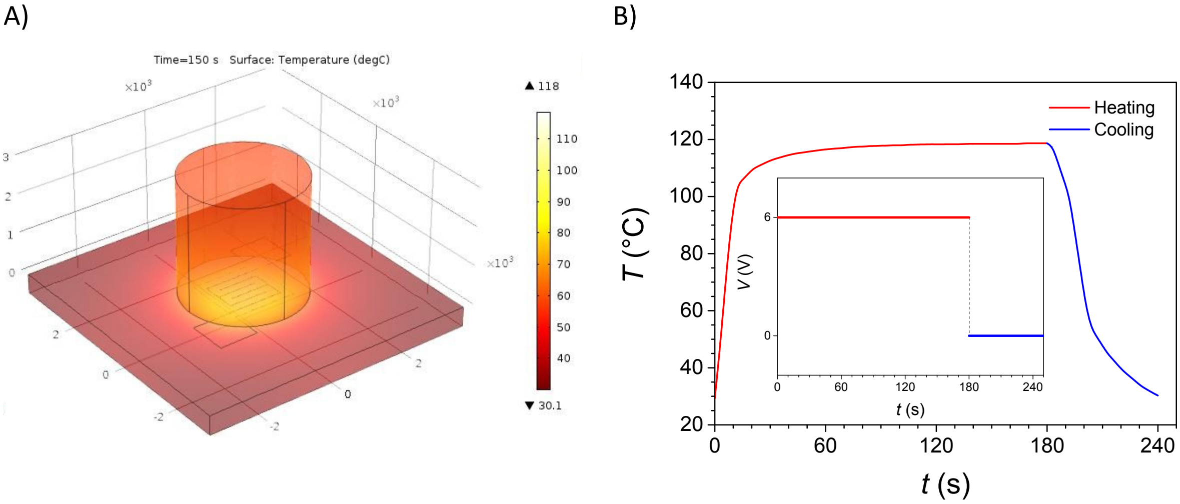

Figure ESI-modelling-2. (A) Temperature distribution along the LCE micropillar obtained by Finite Element Modeling, and (B) the corresponding temperature evolution in the central part of the Au-microresistor upon applying a square-wave electrical voltage of 6 V for 3 min.